Ocean tidal signals in observatory and satellite magnetic measurements

S. Maus[1,2,3] and A. Kuvshinov[4,5]

[1] Ocean flow moves sea water through the Earth's magnetic field, inducing electric fields, currents and secondary magnetic fields. These motionally induced magnetic fields have a potential for the remote sensing of ocean flow variability. A first goal must be to gain a better understanding of magnetic field generation by tidal ocean flow. We predict the motionally induced magnetic fields for the six major tidal constituents and compare their amplitudes with the spectra of night time observatory and satellite magnetic measurements for the Indian Ocean. The magnetic variations at the solar S2, K1, and P1 periods turn out to be dominated by unrelated external fields. In contrast, observed lunar M2 and N2 tidal signals are in fair agreement with predictions from motional induction. The lunar diurnal O1 signal, visible at some observatories, could be caused by ocean flow but disagrees in amplitude with our predictions. *INDEX TERMS:* 1594 Geomagnetism and Paleomagnetism: Instruments and techniques; 1545 Geomagnetism and Paleomagnetism: Spatial variations (all harmonics and anomalies); 1515 Geomagnetism and Paleomagnetism: Geomagnetic induction; 4560 Oceanography: Physical: Surface waves and tides (1255). **Citation:** Maus, S., and A. Kuvshinov (2004), Ocean tidal signals in observatory and satellite magnetic measurements, *Geophys. Res. Lett.*, *31*, L15313, doi:10.1029/2004GL020090.

1. Introduction

[2] Sea water is a fairly good electrical conductor. When moved by ocean flow through the Earth's magnetic field, electric fields, currents and secondary magnetic fields are induced. These depend on the geometry and time scales of the ocean flow and on the conductivity of the sea water, the sediments, the crust and the upper mantle [*Sanford*, 1971]. For example, vertical shear in the Gulf Stream generates horizontal magnetic fields in excess of 100 nT at a few hundred meters depth [*Sanford*, 1971; *Lilley et al.*, 2001]. However, such strong toroidal magnetic fields, generated by poloidal electric currents, are confined to the oceans. Poloidal magnetic fields observable by land observatories and satellites are generally much weaker, reaching amplitudes up to a few nT. This is small compared with other contributions to the magnetic field, in particular from the magnetization of the crust. Therefore, ongoing studies focus on time varying

flows, such as the tides, seasonal variations, the El Niño/ Southern Oscillation (ENSO) and Rossby waves [*Tyler et al.*, 1999].

[3] Periodic tidal signals are particularly easy to detect and have been studied extensively using magnetic observatory data [see, e.g., *Malin*, 1970; *McKnight*, 1995]. A problem, however, is the presence of ionospheric tidal dynamo signals. One possibility to separate ionospheric and ocean tides is to use the Chapman-Miller method on the complete time series, assuming that the ionospheric tidal signal vanishes at midnight [*Malin*, 1970]. Another possibility is to discard all day time data and assume that ionospheric currents are negligible on the night side of the Earth, excluding the high latitudes. Indeed, a recent study by *Tyler et al.* [2003] showed that the M2 tidal signal can be mapped from night side CHAMP satellite measurements and is largely in agreement with the motionally induced field predicted from an ocean flow model determined from satellite radar altimetry [*Erofeeva and Egbert*, 2002]. Here, we follow up on these findings by computing predictions for the major tidal constituents S2, M2, N2, K1, P1 and O1 using a more accurate numerical procedure and comparing their amplitudes with the power spectra of night side observatory and satellite magnetic measurements above and around the Indian Ocean.

2. Prediction of Tidal Ocean Flow Signal

[4] To predict the magnetic fields due to tidal ocean flow (Figure 1) we adopt the numerical solution described in *Kuvshinov et al.* [2002] and *Kuvshinov and Olsen* [2004]. It is based on a volume integral equation approach and simulates the electromagnetic fields excited by arbitrary sources in three-dimensional (3-D) spherical models of electric conductivity. These 3-D models consist of a number of anomalies of conductivity $\sigma_{3D}(r, \vartheta, \varphi)$, embedded in a host section of conductivity $\sigma_b(r)$. Here ϑ, φ and r are colatitude, longitude and the distance from the Earth's center, respectively. Within this approach Maxwell's equations in the frequency domain,

$$\nabla \times \mathbf{H} = \sigma \mathbf{E} + \mathbf{j}^{ext} \qquad (1)$$

$$\nabla \times \mathbf{E} = i\omega\mu_o \mathbf{H} \qquad (2)$$

are reduced to a scattering equation solved by the bi-conjugate gradient method. Here, $\mathbf{j}^{ext}$ is the exciting current, time-harmonic dependency is $e^{-i\omega t}$, μ_o is the magnetic permeability of free space, $i = \sqrt{-1}$, $\omega = 2\pi/T$ is the angular frequency, T is the period of variations, σ is the conductivity distribution in the model. Once the scattering equation is solved (and thus the electric field at depths

---

[1]CIRES, University of Colorado, Boulder, Colorado, USA.
[2]Also at National Geophysical Data Center, National Oceanic and Atmospheric Administration, Boulder, Colorado, USA.
[3]On leave from GeoForschungsZentrum Potsdam, Potsdam, Germany.
[4]Danish Space Research Institute, Copenhagen, Denmark.
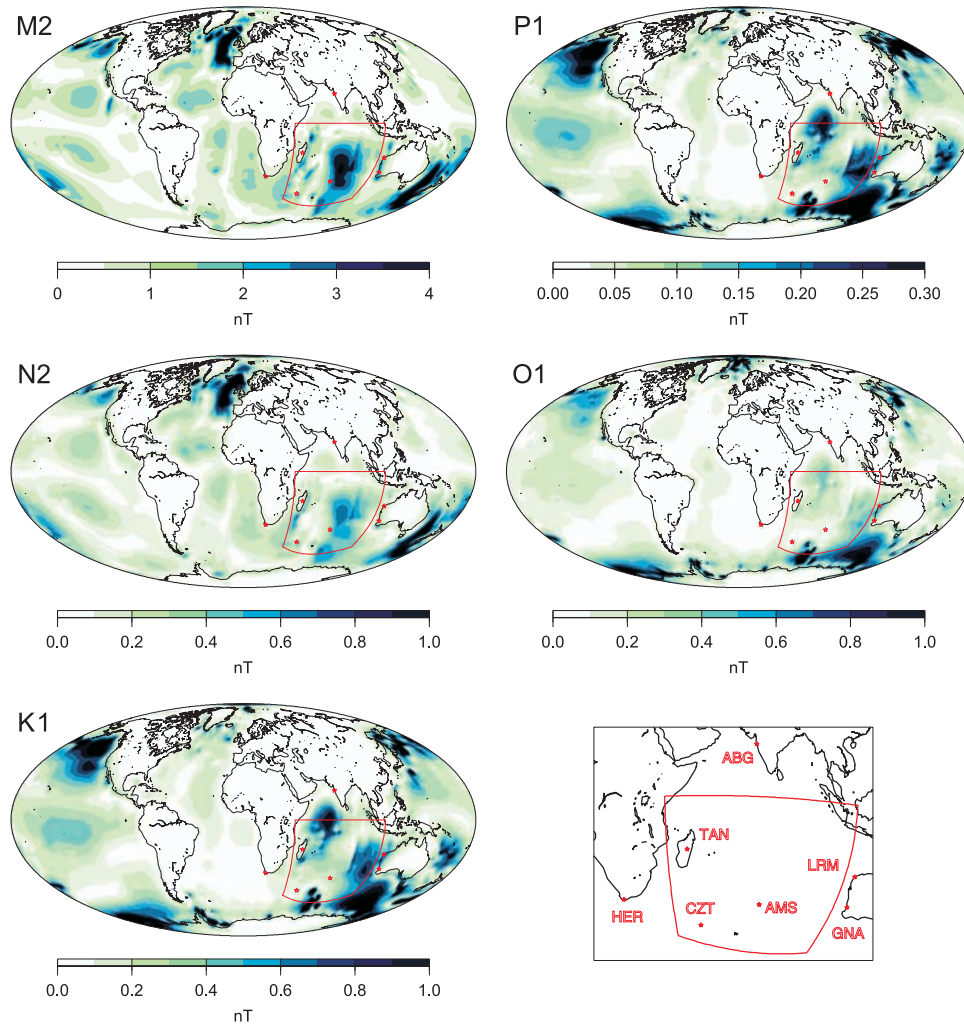[5]On leave from Geoelectromagnetic Research Institute, Troitsk, Russia.

Figure 1. Predicted amplitude of the vertical component of the magnetic field at ground level for the five strongest tidal constituents. S2 is not shown because it is masked by the daily variation of the geomagnetic field. Magnetic observatories used in this study are indicated as red stars, while the rectangle indicates the region for which CHAMP satellite measurements were analyzed.

occupied by 3-D anomalies is determined), the magnetic field **H**, at the observation points $\mathbf{r} \in V^{obs}$ is calculated as

$$\mathbf{H} = \int_{V^{ext}} G_b^h(\mathbf{r}, \mathbf{r}')\mathbf{j}^{ext}(\mathbf{r}')dv' + \int_{V^{mod}} G_b^h(\mathbf{r}, \mathbf{r}')\mathbf{j}^q(\mathbf{r}')dv', \quad (3)$$

where $\mathbf{j}^q = (\sigma - \sigma_b)\mathbf{E}$, G_b^h is the "magnetic" Green's tensor of the host radially-symmetric section (the explicit expressions to calculate the elements of Green's tensor are given in *Kuvshinov et al.* [2002]), V^{ext} and V^{mod} are the spherical layers which comprise the exciting current $\mathbf{j}^{ext}$ and the 3-D anomalies, respectively. Note that in our problem statement, the 3-D model consists of a surface spherical shell of conductance $S(\theta, \varphi)$ underlain by a radially symmetric conductor, and $\mathbf{j}^{ext}$ degenerates to the current density $\mathbf{J}^{ext}$, which is calculated as

$$\mathbf{J}^{ext} = \sigma_w(\mathbf{U} \times \mathbf{B}^m), \quad (4)$$

where $\sigma_w = 3.2$ S/m is the mean sea water conductivity, **U** is depth integrated velocity due to ocean tides, taken from the TPXO.6.1 global tidal model [*Erofeeva and Egbert*, 2002], and $\mathbf{B}^m$ is the main magnetic field derived from IGRF 2000.

All the simulations are made on a mesh with a spatial resolution of $1° \times 1°$. The shell conductance $S(\theta, \varphi)$ accounts for contributions from the sea water and from the sediments. The conductance of the ocean layer is derived from the global $5' \times 5'$ NGDC/NOAA's ETOPO bathy-
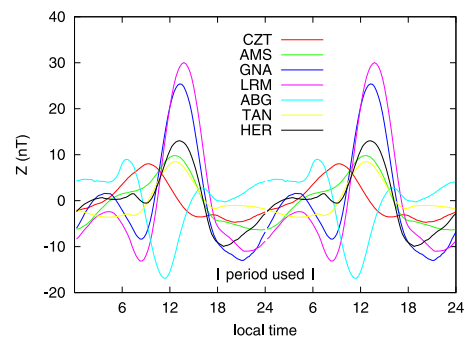

Figure 2. Average daily variations at the 7 observatories used in this study (see Figure 1 for observatory locations). The selected night time period avoids external fields caused by ionospheric currents.
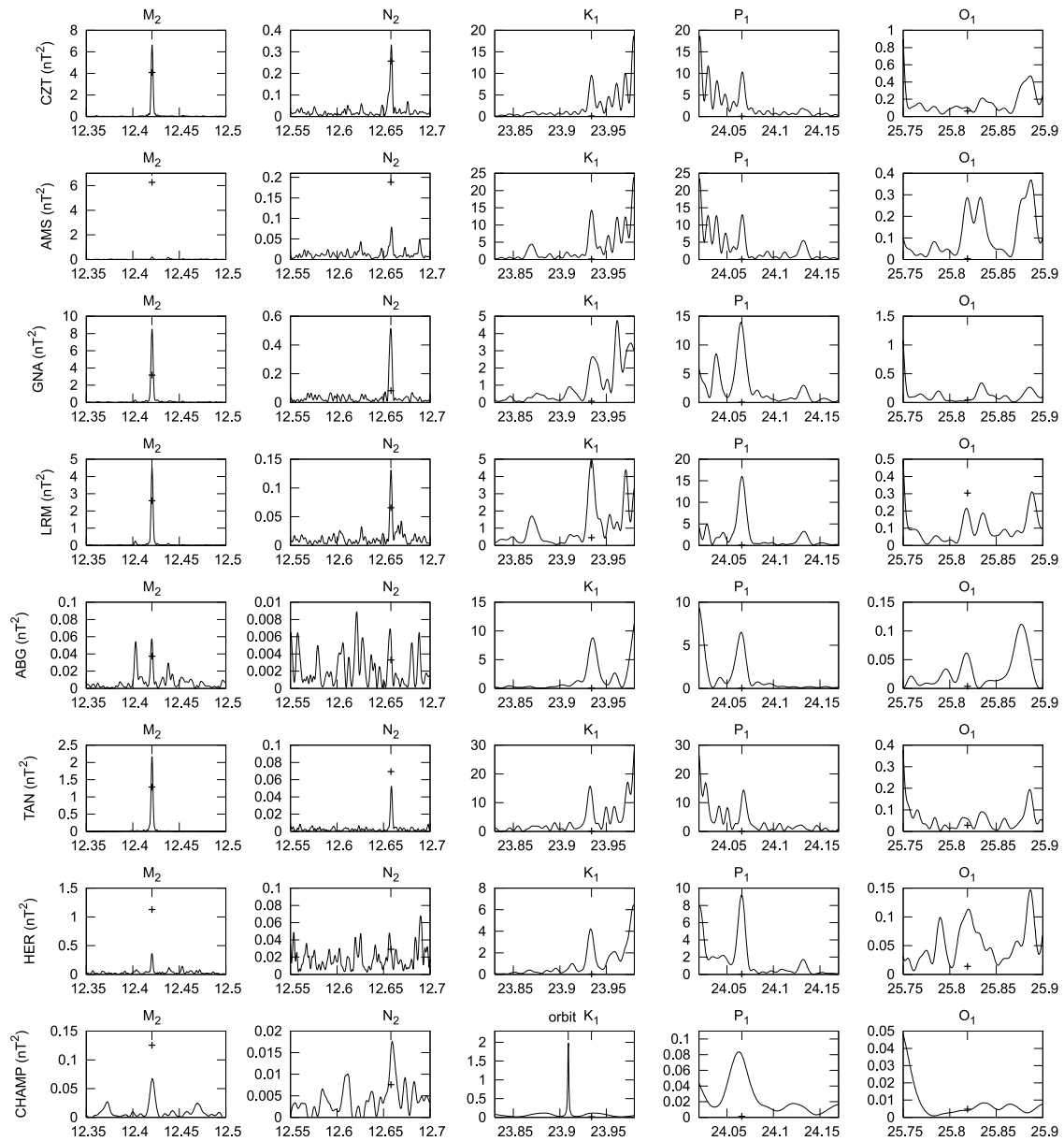
Figure 3. Power spectra of the Z component of observatory magnetic field measurements in and around the Indian Ocean. The bottom row shows the corresponding spectra for the total intensity anomaly measured by the CHAMP satellite at around 400 km altitude, after subtracting a white noise level of 0.01 nT^2. A sharp peak near the K1 period corresponds to the rotation of the orbital plane, indirectly sampling the daily magnetic variations. The "+" indicates our prediction for the squared amplitude of the ocean tidal signal.

metry, multiplying the water depth by σ_w. The conductance of the sediments is calculated from the global sediment thickness given by the 1° × 1° map of *Laske and Masters* [1997] with the use of a heuristic procedure similar to that described in *Everett et al.* [2003]. For the underlying spherical conductor we choose a 4-layer Earth section consisting of a 100 km resistive lithosphere with 3000 Ωm followed by a moderately resistive layer of 70 Ωm down to 500 km, a second transition layer of 16 Ωm from 500 km to 750 km, and an inner uniform sphere of 0.42 Ωm.

3. Observed Magnetic Signal Power

[5] The present study is limited to night time observatory and satellite magnetic measurements. Since the usual Fou-

rier techniques are not applicable to incomplete time series, we directly fitted a 3 parameter model

$$M(t) = M_0 + M_r \cos \omega t + M_i \sin \omega t, \qquad (5)$$

to the observations in order to determine the power $M_i^2 + M_r^2$ as a function of frequency ω. The Indian Ocean was chosen as a study area since all tidal constituents are relatively strong in this region.

3.1. Observatory Data

[6] From the minute data of seven observatories (Figure 1), located on islands and on the coasts of the Indian Ocean, we subtracted the long term trend and then computed the daily variation (Figure 2). The selected period of 18 to 6 local time

(LT) is seen to be comparatively quiet. In fact, one observatory, Port au Francais (PAF), showed significant night time variations (at $-49.4°$ latitude possibly already too close to the southern polar electrojet region) and was therefore excluded from the analysis. Since the Z component of a poloidal field usually contains more information than the individual horizontal components, we limited the analysis to Z. A sliding window of 8 years was moved over each time series in 1 year steps. The powers for each window were then averaged. In the upper seven rows of Figure 3 the observatory power spectra are compared with the numerical predictions for ocean tidal flow.

3.2. Satellite Data

[7] CHAMP (http://op.gfz-potsdam.de/champ) total intensity measurements were selected for 0 to 5 LT and magnetic activity $K_p \leq 2$. The main field model Oersted-10b-03 [Olsen, 2002]) and the crustal field model MF3 [Maus et al., 2002] were subtracted from the data. Then, a filter similar to the one described in Maus et al. [2002] was applied to remove long wavelength magnetospheric fields which are orders of magnitude stronger than the ocean tidal signal. The residuals were then sorted into $8°$ longitude by $5°$ latitude bins. To the data in each bin we individually fit the harmonic model of equation (5), separately for each bin, due to the phase difference between the bins. The powers determined individually for each bin were then averaged and the results are displayed as a function of period in the lower row of Figure 3. The predicted powers, also displayed in Figure 3, were obtained by synthesizing the model predictions along the satellite tracks and processing, filtering and analyzing these predicted signals in the same way as the true observations.

4. Discussion and Outlook

[8] Night time observatory and CHAMP satellite magnetic measurements exhibit clear peaks at the dominant tidal periods. For the solar K1 and P1 tidal periods, the observed signal strengths far exceed the expectations for tidal ocean flow. K1 and P1 periods correspond to the first annual modulation of a diurnal signal. The observed amplitude of a few nT is consistent with the model of an Earth fixed point experiencing daily and seasonal variations in its location relative to a stable magnetospheric field [Maus et al., 2004].

[9] In contrast, observed lunar tidal signals at the M2 and N2 periods are likely to be dominated by ocean flow. The discrepancy of a slightly weaker than predicted satellite M2 signal over the Indian ocean, already pointed out by Tyler et al. [2003], persists despite of using a larger set of CHAMP data, a newer ocean flow model, and a more accurate solution of the induction equation. At surface level, tidal signal strengths are roughly as expected for CZT, ABG and TAN, while they are weaker at AMS and HER, and stronger than expected at GNA an LRM. We have checked that variations in conductivity due to salinity cannot account for the discrepancies. The lunar diurnal O1 tide appears to be visible at AMS, LRM, ABG and HER, although the observed strength deviates significantly from the predictions for tidal ocean flow. Overall, the disagreement between observed lunar tidal signals and the predictions for motional induction in the oceans is very significant. Whether this is due to contamination of the observations by non-ocean tidal signals, shortcomings of the data analysis or inaccuracies in the prediction is presently unknown and should motivate further investigations. As a possible starting point our model predictions and estimated power spectra are available at http://www.gfz-potsdam.de/pb2/pb23/SatMag/ocean_tides.html.

References

Erofeeva, S., and G. Egbert (2002), Efficient inverse modelling of barotropic ocean tides, J. Atmos. Oceanic Technol., 19, 183–204.
Everett, M., S. Constable, and C. Constable (2003), Effects of near-surface conductance on global satellite induction responses, Geophys. J. Int., 153, 277–286.
Kuvshinov, A., and N. Olsen (2004), 3-D modelling of the magnetic fields due to ocean tidal flow, CHAMP Mission Results II, Springer Berlin, 359–65.
Kuvshinov, A., D. Avdeev, O. Pankratov et al. (2002), Modelling electromagnetic fields in 3D spherical Earth using fast integral equation approach, in 3D Electromagnetics, edited by M. S. Zhdanov and P. E. Wannamaker, chap. 3, pp. 43–54, Elsevier Sci., New York.
Laske, G., and G. Masters (1997), A global digital map of sediment thickness, EOS Trans. AGU, 78(46), Fall Meet. Suppl., F483.
Lilley, F. E. M., A. White, and G. S. Heinson (2001), Earth's magnetic field: Ocean current contributions to vertical profiles in deep oceans, Geophys. J. Int., 147, 163–175.
Malin, S. R. C. (1970), Separation of lunar daily variations into parts of ionospheric and oceanic origin, Geophys. J. R. Astron. Soc., 21, 447–455.
Maus, S., M. Rother, R. Holme et al. (2002), First scalar magnetic anomaly map from champ satellite data indicates weak lithospheric field, Geophys. Res. Lett., 29(14), 1702, doi:10.1029/2001GL013685.
Maus, S., H. Lühr, G. Balasis, M. Rother, and M. Mandea (2004), Introducing POMME, the Potsdam Magnetic Model of the Earth, CHAMP Mission Results II, Springer Berlin, 293–298.
McKnight, J. D. (1995), Lunar daily variations in New Zealand, Geophys. J. Int., 122, 889–898.
Olsen, N. (2002), A model of the geomagnetic main field and its secular variation for epoch 2000 estimated from Ørsted data, Geophys. J. Int., 149, 454–462.
Sanford, T. B. (1971), Motionally induced electric and magnetic fields in the sea, J. Geophys. Res., 76, 3476–3492.
Tyler, R. H., J. M. Oberhuber, and T. B. Sanford (1999), The potential for using ocean generated electromagnetic fields to remotely sense ocean variability, Phys. Chem. Earth A, 24, 429–432.
Tyler, R., S. Maus, and H. Lühr (2003), Satellite observations of magnetic fields due to ocean tidal flow, Science, 299, 239–241.
Wessel, P., and W. H. F. Smith (1991), Free software helps map and display data, EOS Trans. AGU, 72, 441, 445–446.

————————————
A. V. Kuvshinov, Danish Space Research Institute, Juliane Maries Vej 30, DK-2100 Copenhagen Ø, Denmark.
S. Maus, National Geophysical Data Center, NOAA E/GC1, 325 Broadway, Boulder, CO 80305-3328, USA. (stefan.maus@noaa.gov)